

Magnetic Field Induced Non-Fermi-Liquid Behavior in YbAgGe Single Crystal

S. L. Bud'ko*, E. Q. T. Morosan*[†], and P. C. Canfield*[†]

**Ames Laboratory and* [†]*Department of Physics and Astronomy,*
Iowa State University, Ames, IA 50011, USA

(Dated: November 17, 2018)

Abstract

Detailed anisotropic resistivity and heat capacity measurements down to ~ 0.4 K and up to 140 kOe are reported for a single crystalline YbAgGe. Based on these data YbAgGe, a member of the hexagonal RAgGe series, can be classified as new, *stoichiometric* heavy fermion compound with two magnetic ordering temperatures below 1 K and field-induced non-Fermi-liquid behavior above 45-70 kOe and 80-110 kOe for $H \parallel (ab)$ and $H \parallel c$ respectively.

PACS numbers: 75.30.Mb, 75.30.Kz

I. INTRODUCTION

YbAgGe is the penultimate member of the hexagonal RAgGe series [1] and was recently identified [1, 2, 3, 4] as a new Yb-based heavy fermion compound. Magnetization measurements on YbAgGe down to 1.8 K [1] show moderate anisotropy (at low temperatures $\chi_{ab}/\chi_c \approx 3$) and a loss of local moment character below ~ 20 K (Fig. 1). The in-plane $M(H)$ at $T = 2$ K shows a trend toward saturation whereas $H \parallel c$ field-dependent magnetization continues to be virtually linear below 140 kOe (Fig. 1, inset). Initial thermodynamic and transport measurements down to 0.4 K [1, 2, 3] reveal two magnetic transitions, a higher one at ≈ 1 K, and a lower one, with very sharp features in $\rho(T)$ and $C_p(T)$, at ≈ 0.65 K (Fig. 2). Given that the magnetic entropy inferred from the Fig. 2 is only $\sim 5\%$ of $R \ln 2$ at 1 K and only reaches $R \ln 2$ by ~ 25 K it seems likely that these transitions are associated with a small moment ordering. Based on these measurements the compound was anticipated to be close to the quantum critical point. The linear component of $C_p(T)$, γ , is ~ 150 mJ/mol K² between 12 K and 20 K. $C_p(T)/T$ rises up to ~ 1200 mJ/mol K² for $T \sim 1$ K but given the presence of the magnetic transitions below 1 K, it is difficult to unambiguously evaluate the electronic specific heat. Grossly speaking, $150 \text{ mJ/mol K}^2 < \gamma < 1 \text{ J/mol K}^2$ leading to an estimate $10 \text{ K} < T_K < 100 \text{ K}$ for the Kondo temperature, T_K .

Since the number of the Yb-based heavy fermion compounds is relatively small [5, 6, 7] any new member of the family attracts attention [6, 8]. As an up to date example, YbRh₂Si₂, a heavy fermion antiferromagnet [9], became a subject of intensive, rewarding exploration [10, 11, 12]. The case of YbAgGe appears to have the potential of being somewhat similar to YbRh₂Si₂: the relatively high value of γ and the proximity of the magnetic ordering temperature to $T = 0$ suggest that YbAgGe is close to a quantum critical point (QCP) and make it a good candidate for a study of the delicate balance and competition between magnetically ordered and strongly correlated ground states under the influence of a number of parameters such as pressure, chemical substitution and/or magnetic field.

In this work we report the magnetic-field-induced evolution of the ground state of YbAgGe as seen in anisotropic resistivity and specific heat measurements up to 140 kOe. We show that on increase of the applied magnetic field the progression from small moment magnetic order to QCP with the evidence of non-Fermi-liquid (NFL) behavior and, in higher fields, to low temperature Fermi-liquid (FL) state is observed.

II. EXPERIMENTAL

YbAgGe crystallizes in hexagonal ZrNiAl-type structure [13, 14]. YbAgGe single crystals in the form of clean hexagonal cross section rods of several mm length and 0.3-0.8 mm² cross section were grown from high temperature ternary solutions rich in Ag and Ge. Their structure and the absence of impurity phases were confirmed by powder X-ray diffraction (see [1] for details of the samples' growth). Temperature and field dependent resistivity $\rho(H, T)$ and heat capacity $C_p(H, T)$ were measured down to 0.4 K in an applied magnetic field up to 140 kOe in a Quantum Design PPMS-14 instrument with He-3 option. For resistivity a standard ac four probe resistance technique ($f = 16$ Hz, $I = 1$ -0.3 mA) was used. Pt leads were attached to the sample with Epotek H20E silver epoxy so that the current was flowing along the crystallographic c axis. For these measurements the magnetic field was applied in two directions: in (ab) plane, approximately along $[1\bar{2}0]$ direction (transverse, $H \perp I$, magnetoresistance) and along c -axis (longitudinal, $H \parallel I$ magnetoresistance). For heat capacity measurements a relaxation technique with fitting of the whole temperature response of the microcalorimeter was utilized. The background heat capacity (sample platform and grease) was measured for all necessary (H, T) values and was accounted for in the final results. $C_p(H, T)$ was also measured with the field along the c -axis and in the (ab) plane (the same orientations as in $\rho(H, T)$ data). The heat capacity of LuAgGe was measured in the same temperature range and was used to estimate a non-magnetic contribution to the heat capacity of YbAgGe.

III. RESULTS

A. $H \parallel (ab)$

The low temperature part of the temperature dependent resistivity measured in various constant magnetic fields applied in the (ab) plane is shown in Fig. 3(a). There are several features that apparently require detailed examination. Multiple transitions in zero field is a feature that is common throughout the RAgGe series [1] and in the case of YbAgGe in zero field in addition to the sharp transition at approximately 0.64 K another, albeit less pronounced feature is apparent at ~ 1 K. Whereas the 0.64 K transition seems to be pushed below the base temperature of our measurements by a 20 kOe field, the other feature shifts

down in temperature more gradually and is seen up to 40 kOe. For applied field between 60 and 90 kOe (Fig. 3(c)) low temperature $\rho(T)$ functional dependence is linear down to our base temperature, with the upward curvature in $\rho(T)$ starting to occur below ~ 0.8 K in 100 kOe field. In higher applied fields ($H \geq 100kOe$) (Fig. 3(d)) low temperature resistivity follows $\rho(T) = \rho_0 + AT^2$ (Fermi-liquid-like) functional behavior with the range of its occurrence (for each curve the upper limit is marked with arrow in Fig. 3(d)) increasing with the increase of applied field and the coefficient A decreasing.

Field dependent resistivity data taken at constant temperatures between 0.4 K and 5.0 K are shown in Fig. 4(a). At $T = 0.4$ K two fairly sharp features, at ~ 13 kOe and ~ 40 kOe are seen in the $\rho(H)$ data. The lower field feature may be identified as a signature of a metamagnetic transition between two different magnetically ordered phases. This feature vanishes as the temperature increased to $T > 0.65$ K (Fig. 4(b)). The second, more smoothed, higher field feature, may be to a transition from a magnetically ordered state to a saturated paramagnetic state. If the critical field for this transition is inferred from the maximum in $\rho(H)$, this transition can be discerned up to 0.8-0.9 K (Fig. 4(b)), consistent with it being associated with the ~ 1 K transition seen in the $H = 0$ $\rho(T)$ and $C_p(T)$ data (Fig. 2). At higher temperatures (Fig. 4(a)) this feature broadens and resembles a crossover rather than a transition. For $2 \text{ K} < T < 5 \text{ K}$ $\rho(H)$ looks like a generic magnetoresistance of a paramagnetic metal [15]. The large black dots in Fig. 4(b) show the evolution of the two aforementioned features.

The low temperature heat capacity of YbAgGe is shown for several values of applied magnetic field in Fig. 5(a). The lower temperature, sharp peak is seen only for $H = 0$, having been suppressed below the base temperature by an applied field of 20 kG. The higher temperature maximum seen just below 1 K (for $H = 0$) shifts down with the increase of the applied field and drops below 0.4 K for $H \geq 60kOe$. The field dependence of this feature is consistent with that of the higher temperature feature in resistivity discussed above giving further evidence that YbAgGe has two closely-spaced magnetic transitions. The same data plotted as C_p/T vs T^2 (Fig. 5(b)) allow for the tracking of the variation of the electronic specific heat coefficient γ in applied field (for $H \geq 60$ kOe, when the magnetic order is suppressed). The values at $T^2 = 0.35 \text{ K}^2$ (a value chosen to avoid the upturn in lowest temperature, highest field $C_p/T(T^2)$ data possibly associated with the nuclear Schottky contribution) give a reasonable approximation of $\gamma(H)$. A more than four-fold decrease of

γ is observed from 60 kOe to 140 kOe.

The magnetic contribution to the YbAgGe specific specific heat (defined as $C_{magn} = C_p(\text{YbAgGe}) - C_p(\text{LuAgGe})$) is shown in Fig. 5(c) in C_{magn}/T vs $\lg T$ coordinates. (It should be noted that $C_p(T)$ of LuAgGe was measured at $H = 0$ and 140 kOe and found to be insensitive to the applied field in this temperature range.) For intermediate values of applied field there is a region of the logarithmic divergency seen in the specific heat data $C_{magn}/T \propto -\ln T$. The largest range of the logarithmic behavior (more than an order of magnitude in temperature, from below 1 K to above 10 K) is observed for $H = 80$ kOe. These data can be described as $C_{magn}/T = \gamma'_0 \ln(T_0/T)$ with $\gamma'_0 \approx 144$ mJ/mol K² and $T_0 \approx 41$ K. These parameters are of the same order of magnitude as those reported for YbRh₂Si₂ [9]. In higher fields Fermi-liquid-like behavior apparently recovers, in agreement with the resistivity data.

The crossover function $(C(H) - C(H = 0))/T$ vs H/T^β ($\beta = 1.15$) (one of the expressions considered in the scaling analysis at a QCP) is shown in the inset to Fig. 5(c). Data for $H \geq 60$ kOe collapse onto one universal curve. Such scaling behavior [16] with β between 1.05 and 1.6 was observed for a number of materials that demonstrate NFL properties [9, 17, 18, 19, 20] and may be considered as further corroboration of the proximity of YbAgGe to a QCP.

B. $H \parallel c$

YbAgGe manifests an easy plane anisotropy in both its low-field and high-field magnetization (Fig. 1). This is a trend that evolves across the RAgGe series [1], *e.g.* in TmAgGe the local moments are extremely anisotropic being confined to the basal plane. Not surprisingly this anisotropy manifests itself in the low-temperature $\rho(H, T)$ and $C_p(H, T)$ data. The variation of the temperature dependent resistivity for $H \parallel c$ (Fig. 6(a)) is comparable to that for $H \parallel (ab)$. As for the in-plane orientation of the field, the two transitions seen for $H = 0$ move to lower temperatures with application of magnetic field, albeit the effect of field is weaker, so that the lower temperature transition is still being detected as a break in slope for $H = 20$ kOe whereas the higher temperature transition persists up to 80 kOe (Fig. 6(b)). The field range for which linear, low temperature resistivity can be seen is smaller and is shifted to higher fields (Fig. 6(c)), whereas the $\rho - \rho_0 \propto T$ behavior can be recognized

for $H = 100$ kOe and 120 kOe, and a slight upward curvature above 0.4 K is already seen at $H = 130$ kOe. The low temperature resistivity can be characterized by $\rho(T) = \rho_0 + AT^2$ (Fig. 6(d)) and this curvature can be viewed as a signature of a FL behavior. The range of T^2 behavior increases and the value of A decreases with an increase of applied field. The field-dependent resistivity for this orientation of the magnetic field (Fig. 7(a)) is similar to the set of $\rho(H)$ isotherms for $H \parallel (ab)$ except for the weaker field dependence of the observed transitions (Fig. 7(b)).

The low temperature part of the heat capacity measured for $H \parallel c$ up to 140 kOe is shown in Fig. 8(a). Upper magnetic ordering transition temperature decreases with increase of applied field and can be followed up to 60 kOe. Electronic contribution to the specific heat for fields where the ordering transition is suppressed can be estimated from the Fig. 8(b). For this orientation the largest range of the logarithmic behavior $C_{magn}/T \propto -\ln T$ is observed for $H = 140$ kOe (Fig. 8(c)) and these data can be expressed as $C_{magn}/T = \gamma' \ln(T_0/T)$ with $\gamma' \approx 143$ mJ/mol K² and $T_0 \approx 44$ K, the values of γ' and T_0 being, within the accuracy of the data and the fit, the same as for $H \parallel (ab)$. Scaling behavior of the specific heat data plotted as $(C(H) - C(H = 0))/T$ vs H/T^β (the value of the exponent $\beta = 1.15$ is the same as for $H \parallel (ab)$) is observed for $H \geq 100$ kOe (Fig. 8(c), inset).

IV. SUMMARY AND DISCUSSION

For both sets of data ($H \parallel (ab)$ and $H \parallel c$), at high enough applied fields, long range magnetic order is suppressed, and the electronic contribution to the specific heat can be estimated, whereas the low temperature resistivity shows $\Delta\rho \propto AT^2$ FL-like behavior. The values of γ were estimated at $T^2 = 0.35$ K² ($T \approx 0.6$ K) and decrease with the increasing magnetic field (Fig. 9(a)) in a manner similar to what was observed in YbRh₂Si₂ [10] and other materials. Although the data set is sparse, it is worth noting that an approximately 50-55 kOe shift down of the data for $H \parallel c$ (Fig. 9(a)) brings it into rough agreement with the $H \parallel (ab)$ data and so that the two sets form a universal curve. The T^2 coefficient of FL-like resistivity, A , also decreases with an increase of applied field (Fig. 9(b)). The shift required to have the A data for the two H orientations on the same curve is 30-25 kOe. The field dependence of the Kadowaki-Woods ratio, A/γ^2 [21] is presented in Fig. 9(c). Many of the γ and A values were reckoned for the same magnetic field. In some cases when additional

values of A were available a straightforward interpolation of $\gamma(T)$ was used. Although more data points may be required to clarify these trends, several features are seen in the Fig. 9: the obtained values of A/γ^2 are of the same order of magnitude, but several times higher than $\sim 1 \times 10^{-5} \mu\Omega \text{ cm}/(\text{mJ/mol K})^2$ obtained in [21] and corroborated by the larger set of data in [22, 23]; for $H \parallel (ab)$ the Kadowaki-Woods ratio decreases with an increase of the field (not enough data is available for $H \parallel c$). Though magnetotransport measurements down to lower temperatures will allow for the estimate of A in a wider temperature range and may refine our A/γ^2 data, both of the features seen in Fig. 9(c) were observed in YbRh_2Si_2 [12] and apparently are common for materials where NFL behavior can be induced by magnetic field. In addition, a larger value of the Kadowaki-Woods ratio is anticipated theoretically in the close vicinity of a magnetic instability [24], in agreement with our experimental data, whereas constant (*i.e.* field-independent in our case) Kadowaki-Woods ratio is expected only in the local critical regime [25].

Finally, based on the thermodynamic and transport data down to ~ 0.4 K and up to 140 kOe, we can construct tentative $T - H$ phase diagrams for the two orientations of the applied magnetic field (Fig. 10). Both phase diagrams are very similar. Initially increasing magnetic field drives first the lower and then the higher magnetic transitions to zero. With further increase in field signatures of the NFL behavior appear in the temperature dependent resistivity ($\Delta\rho \propto T$) and heat capacity ($C_{\text{magn}}/T \propto -\ln T$) and at our highest applied field values FL-like low temperature resistivity ($\Delta\rho \propto T^2$) (*i.e.* the coherence line [25, 26] on the $T - H$ phase diagram) is observed. Although the current lack of data below ~ 0.4 K impairs our ability to fully delineate the critical field that corresponds to $T = 0$ QCP, a rather crude assessment of the data (Fig. 10) suggests $H_c^{ab} \approx 45\text{-}70$ kOe, $H_c^c \approx 80\text{-}110$ kOe.

V. CONCLUSIONS

We presented results that allow for the classification of YbAgGe as a new heavy fermion material with magnetic field induced NFL behavior (critical fields are $H_c^{ab} \approx 45\text{-}70$ kOe, $H_c^c \approx 80\text{-}110$ kOe). Although its critical fields are somewhat higher than found for the extensively studied YbRh_2Si_2 , they are still within the range accessible by many groups. It should be mentioned that only very few *stoichiometric* compounds are known to demonstrate this type of behavior, making YbAgGe an important and interesting addition to the

family of strongly correlated materials. Results of this work can serve as a road map for further studies, delineating further experimental courses: macroscopic (magnetization) and microscopic (neutron diffraction, μ SR, Moessbauer spectroscopy) measurements at low temperatures and in applied field are desirable to clarify the nature of the magnetically ordered states in YbAgGe and their evolution in field; lower temperature ($T < 0.4$ K), detailed thermodynamic and transport measurements in the vicinity of the field-induced QCP would be very helpful for the understanding of the physics of field induced NFL behavior and as a point of comparison with a number of existing theories [27, 28, 29, 30] and with other materials with similar behavior. In addition, as is often the case for materials close to QCP, pressure and doping study may have a great potential in fine tuning of the ground state properties of YbAgGe.

Acknowledgments

Ames Laboratory is operated for the U.S. Department of Energy by Iowa State University under Contract No. W-7405-Eng.-82. This work was supported by the Director for Energy Research, Office of Basic Energy Sciences. S.L.B. thanks M. A. Continentino for useful discussions.

-
- [1] E. Q. T. Morosan, S. L. Bud'ko, P. C. Canfield, M. S. Torikachvili, and A. H. Lacerda, J. Magn. Magn. Mat. (2003), submitted for publication.
 - [2] W. P. Beyermann, P. C. Canfield, S. L. Bud'ko, and A. H. Lacerda, Bull. Amer. Phys. Soc. **43**, 115 (1998).
 - [3] P. C. Canfield, E. Morosan, and S. L. Bud'ko, Bull. Amer. Phys. Soc. **48**, 1373 (2003).
 - [4] K. Katoh, Y. Mano, K. Nakano, G. Terui, Y. Niide, and A. Ochiai, J. Magn. Magn. Mat. **XX**, XXX (XXXX), in press.
 - [5] G. R. Stewart, Rev. Mod. Phys. **56**, 755 (1984).
 - [6] Z. Fisk and M. B. Maple, J. Alloys Comp. **183**, 303 (1992).
 - [7] A. C. Hewson, *The Kondo Problem to Heavy Fermions* (Cambridge University Press, Cambridge, UK, 1993).

- [8] J. D. Thompson and J. M. Lawrence, *Handbook on the Physics and Chemistry of Rare Earths* (Elsevier, Amsterdam, 1994), vol. 19, p. 383, ed. by K. A. Gschneidner *et al.*
- [9] O. Trovarelli, C. Geibel, S. Mederle, C. Langhammer, F. M. Grosche, P. Gegenwart, M. Lang, G. Sparn, and F. Steglich, *Phys. Rev. Lett.* **85**, 626 (2000).
- [10] P. Gegenwart, J. Custers, C. Geibel, K. Neumaier, T. Tayama, K. Tenya, O. Trovarelli, and F. Steglich, *Phys. Rev. Lett.* **89**, 056402 (2002).
- [11] K. Ishida, K. Okamoto, Y. Kawasaki, Y. Kitaoka, O. Trovarelli, C. Geibel, and F. Steglich, *Phys. Rev. Lett.* **89**, 107202 (2002).
- [12] J. Custers, P. Gegenwart, H. Wilhelm, K. Neumaier, Y. Tokiwa, O. Trovarelli, C. Geibel, F. Steglich, C. Pépin, and P. Coleman, *Nature* **424**, 524 (2003).
- [13] B. Gibson, R. Pottgen, R. K. Kremer, A. Simon, and K. R. A. Ziebeck, *J. Alloys Comp.* **239**, 34 (1996).
- [14] R. Pottgen, B. Gibson, and R. K. Kremer, *Zeit. Kristallog.* **212**, 58 (1997).
- [15] K. Yosida, *Phys. Rev.* **107**, 396 (1957).
- [16] A. M. Tselik and M. Reiser, *Phys. Rev. B* **48**, R9887 (1993).
- [17] B. Andracka and A. M. Tselik, *Phys. Rev. Lett.* **67**, 2886 (1991).
- [18] M. Lenkewitz, S. Corsépius, G.-F. v. Blanckenhagen, and G. R. Stewart, *Phys. Rev. B* **55**, 6409 (1997).
- [19] K. Heuser, E.-W. Scheidt, T. Schreiner, and G. R. Stewart, *Phys. Rev. B* **58**, R15959 (1998).
- [20] S. Koerner, E.-W. Scheidt, T. Schreiner, K. Heuser, and G. R. Stewart, *J. Low Temp. Phys.* **119**, 147 (2000).
- [21] K. Kadowaki and S. B. Woods, *Solid State Comm.* **58**, 5075 (1986).
- [22] M. A. Continentino, *Phys. Rep.* **239**, 179 (1994).
- [23] N. Tsujii, K. Yoshimura, and K. Kosuge, *J. Phys.: Cond. Mat.* **15**, 1993 (2003).
- [24] T. Takimoto and T. Moriya, *Solid State Comm.* **99**, 457 (1996).
- [25] M. A. Continentino, *Quantum Scaling in Many-Body Systems* (World Scientific, Singapore, 2001).
- [26] M. A. Continentino, G. Japiassu, and A. Troper, *Phys. Rev. B* **39**, 9734 (1989).
- [27] G. R. Stewart, *Rev. Mod. Phys.* **73**, 797 (2001).
- [28] P. Coleman, C. Pépin, Q. Si, and R. Ramazashvili, *J. Phys.: Cond. Mat.* **13**, R723 (2001).
- [29] Y. G. Pogorelov and V. R. Shaginyan, *Pis'ma Zh. Exp. Teor. Fiz.* **76**, 614 (2003), [*JETP Lett.*,

76 (2003) 532].

[30] M. A. Continentino (2003), cond-mat/0307218.

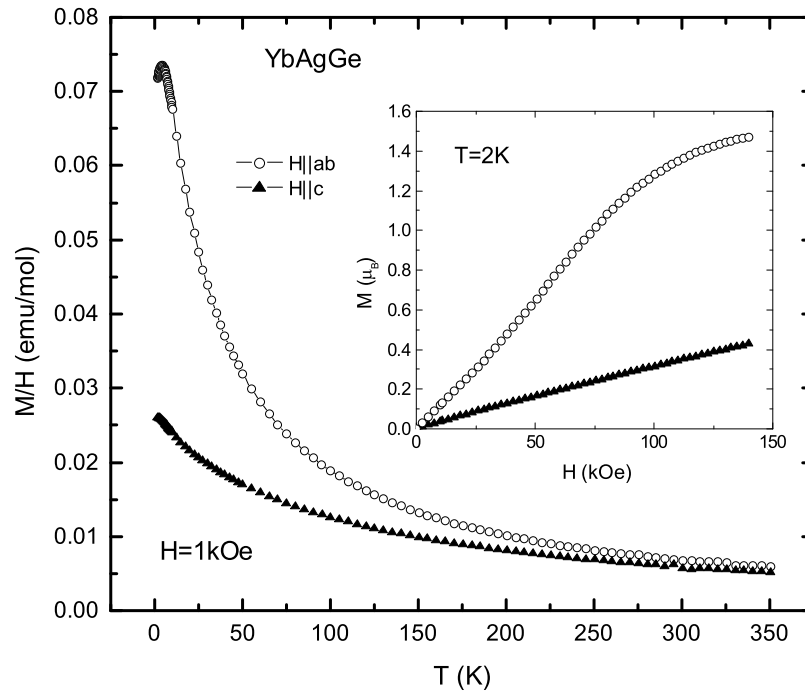


FIG. 1: Anisotropic temperature-dependent DC susceptibility and (inset) field-dependent magnetization of YbAgGe.

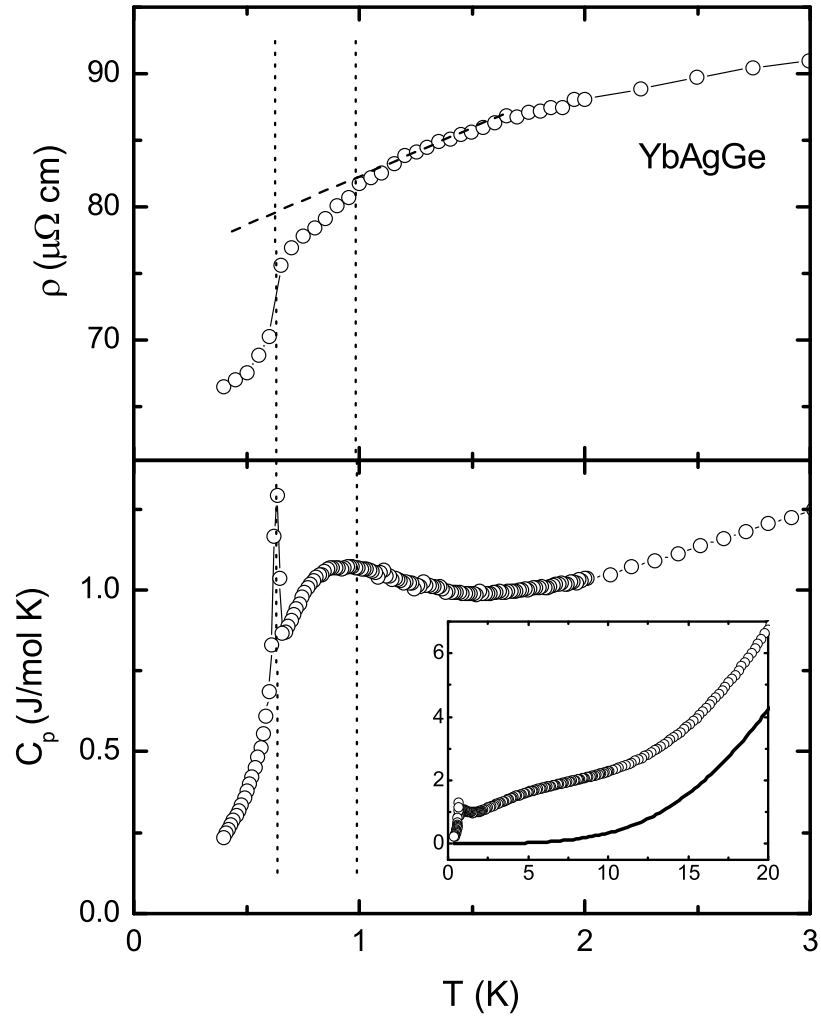


FIG. 2: Low temperature zero field resistivity (upper panel) and specific heat (lower panel) of YbAgGe. Dotted lines point to magnetic transitions. Inset: $C_p(T)$ of YbAgGe and LuAgGe (line) up to 20 K.

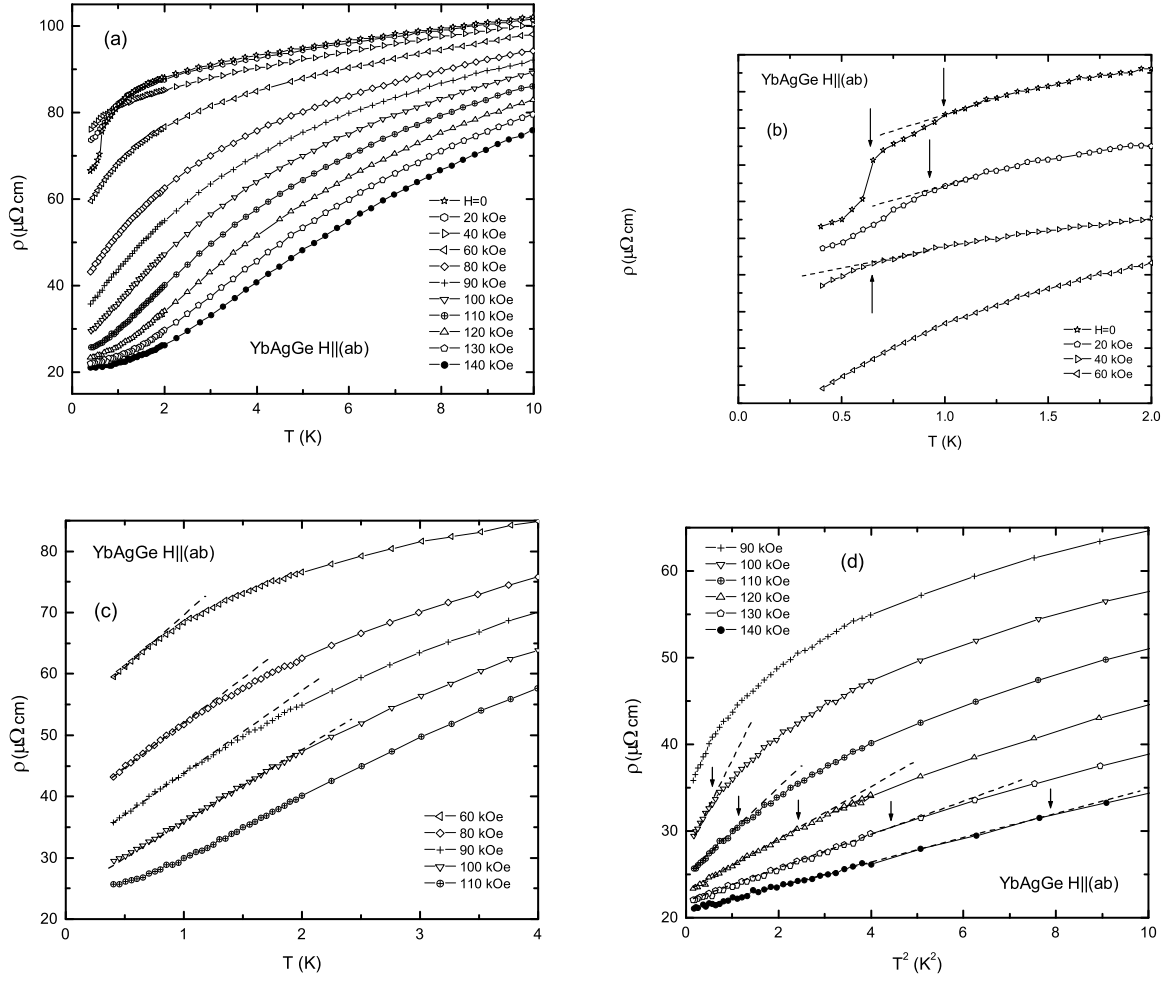


FIG. 3: (a) Low temperature part of $\rho(T)$ curves for YbAgGe taken at different applied fields $H \parallel (ab)$; (b) $\rho(T)$ for $H = 0, 20, 40$ and 60 kOe below 2 K (curves shifted along y axis for clarity), arrows indicate possible magnetic ordering transitions; (c) $\rho(T)$ for $H = 60, 80, 90, 100$ and 110 kOe below 4 K, dashed lines are guides for the eye emphasizing regions of linear $\rho(T)$; (d) resistivity at $H = 90, 100, 110, 120, 130$ and 140 kOe below ~ 3 K as a function of T^2 , dashed lines bring attention to the regions where $\rho(T) = \rho_0 + AT^2$, arrows indicate temperatures at which deviations from T^2 behavior occur.

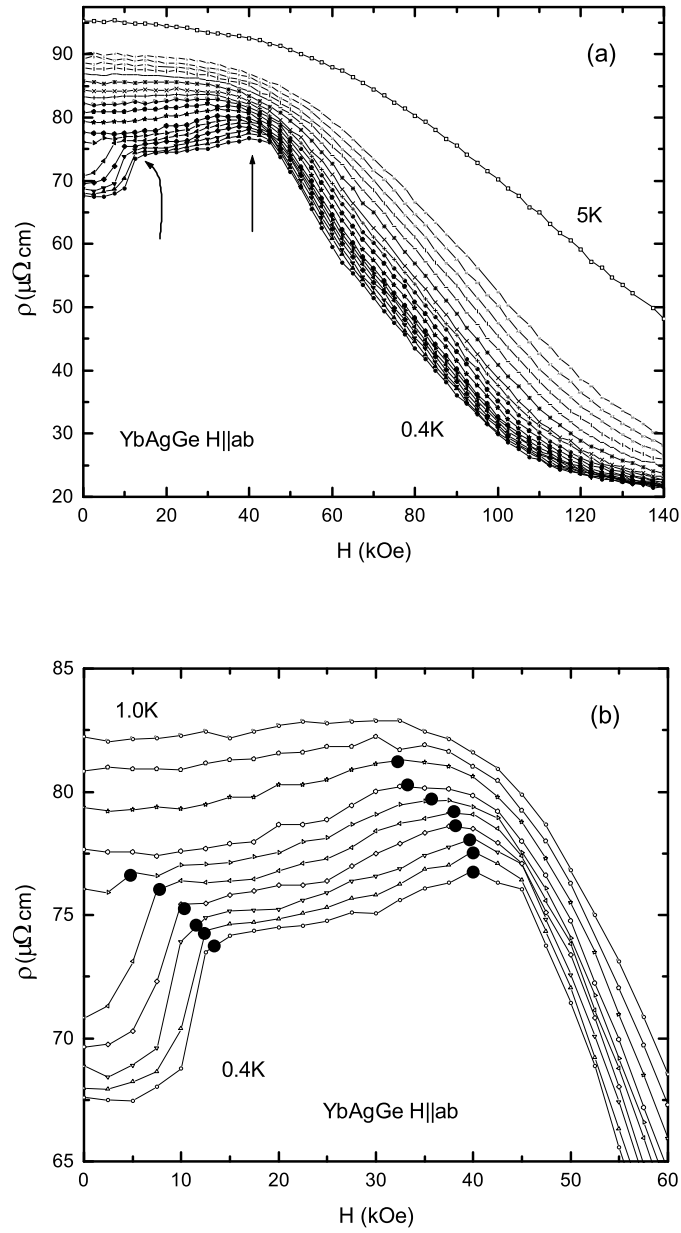


FIG. 4: (a) $\rho(H)$ ($H \parallel (ab)$) isotherms for YbAgGe taken every 0.05 K between 0.4 K and 0.7 K, every 0.1 K between 0.7 K and 1.2 K, every 0.2 K between 1.2 K and 2.0 K and at 2.3 K, 2.5 K and 5.0 K, arrows point to the transitions discussed in the text; (b) enlarged low field - low temperature (0-60 kOe, 0.4-1.0 K) part of the panel (a), black dots mark transitions on the respective curves.

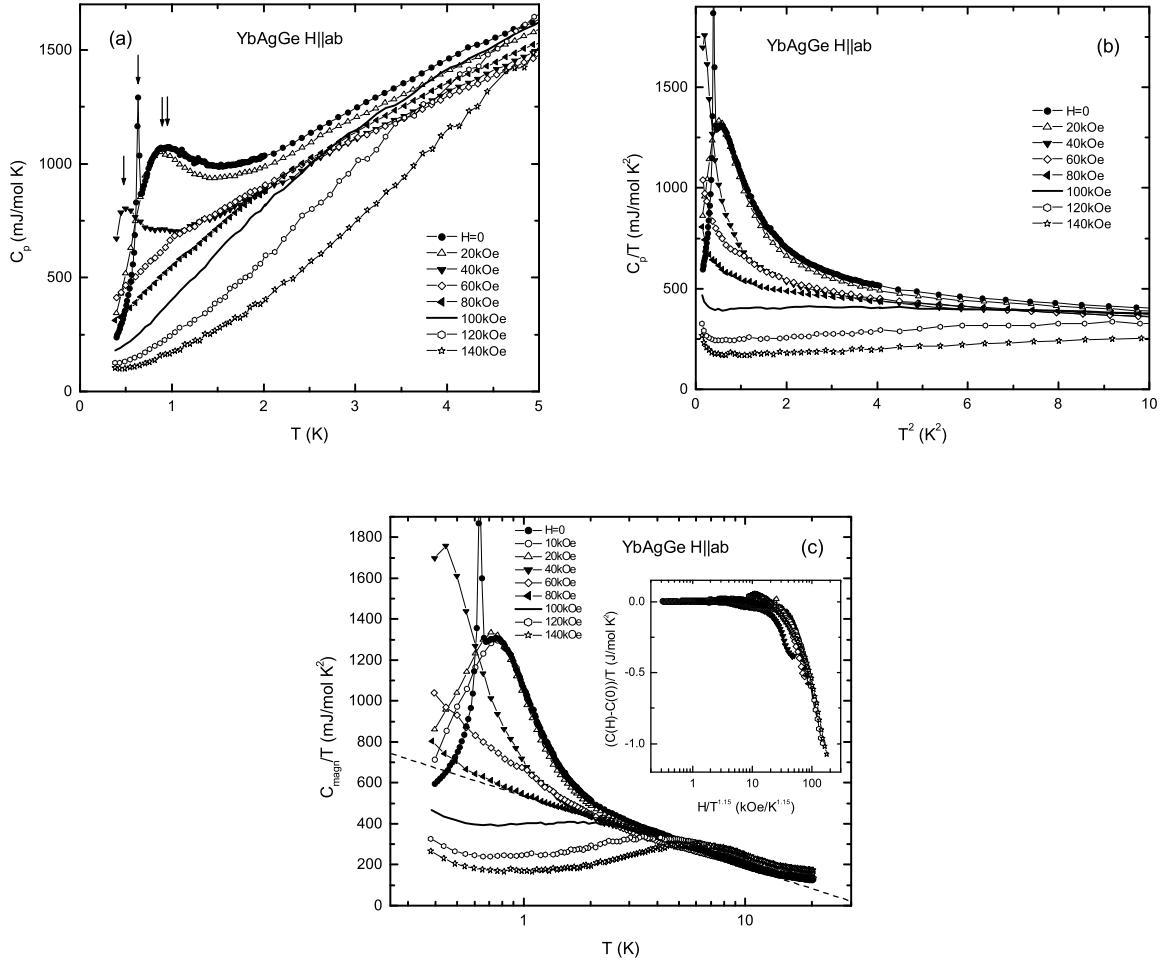


FIG. 5: (a) Low temperature part of the heat capacity curves for YbAgGe taken at different applied fields $H \parallel (ab)$, arrows indicate peaks associated with magnetic ordering; (b) low temperature part of C_p vs T^2 curves; (c) *semi-log* plot of the magnetic part ($C_{\text{magn}} = C_p(\text{YbAgGe}) - C_p(\text{LuAgGe})$) of the heat capacity, C_{magn}/T vs T , for different applied magnetic fields, dashed line is a guide to the eye, it delineates linear region of the $H = 80$ kOe curve; inset: *semi-log* plot of $(C(H) - C(H = 0))/T$ vs $H/T^{1.15}$ ($T \geq 0.8$ K), note approximate scaling of the data for $H \geq 60$ kOe.

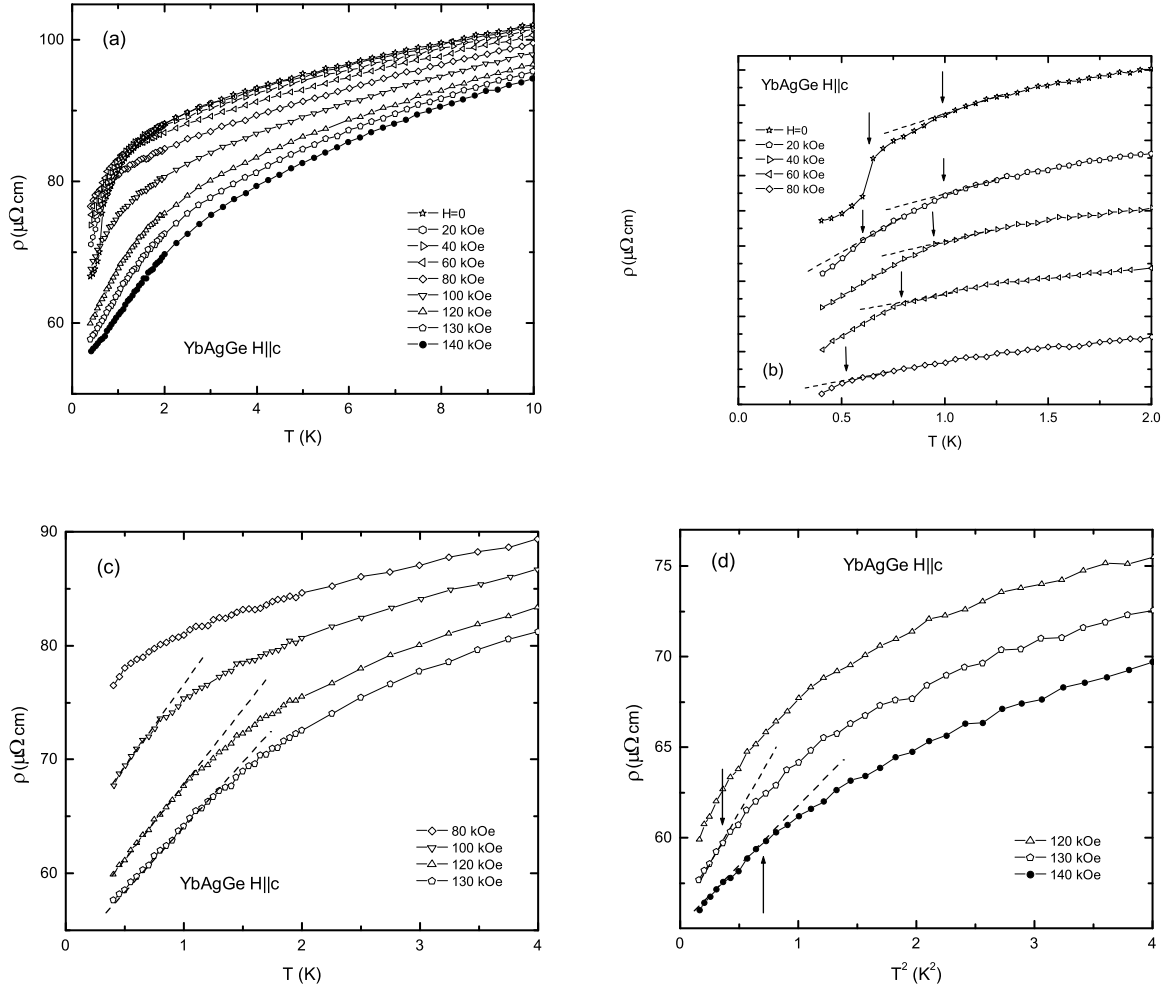


FIG. 6: (a) Low temperature part of $\rho(T)$ curves for YbAgGe taken at different applied fields $H \parallel c$; (b) $\rho(T)$ for $H = 0 - 80$ kOe below 2 K (curves shifted along y axis for clarity), arrows indicate magnetic ordering transitions; (c) $\rho(T)$ for $H = 80, 100, 120$ and 130 kOe below 4 K, dashed lines are guides for the eye emphasizing regions of linear $\rho(T)$; (d) resistivity at $H = 120, 130$ and 140 kOe below ~ 3 K as a function of T^2 , dashed lines bring attention to the regions where $\rho(T) = \rho_0 + AT^2$, arrows indicate temperatures at which deviations from T^2 behavior occur.

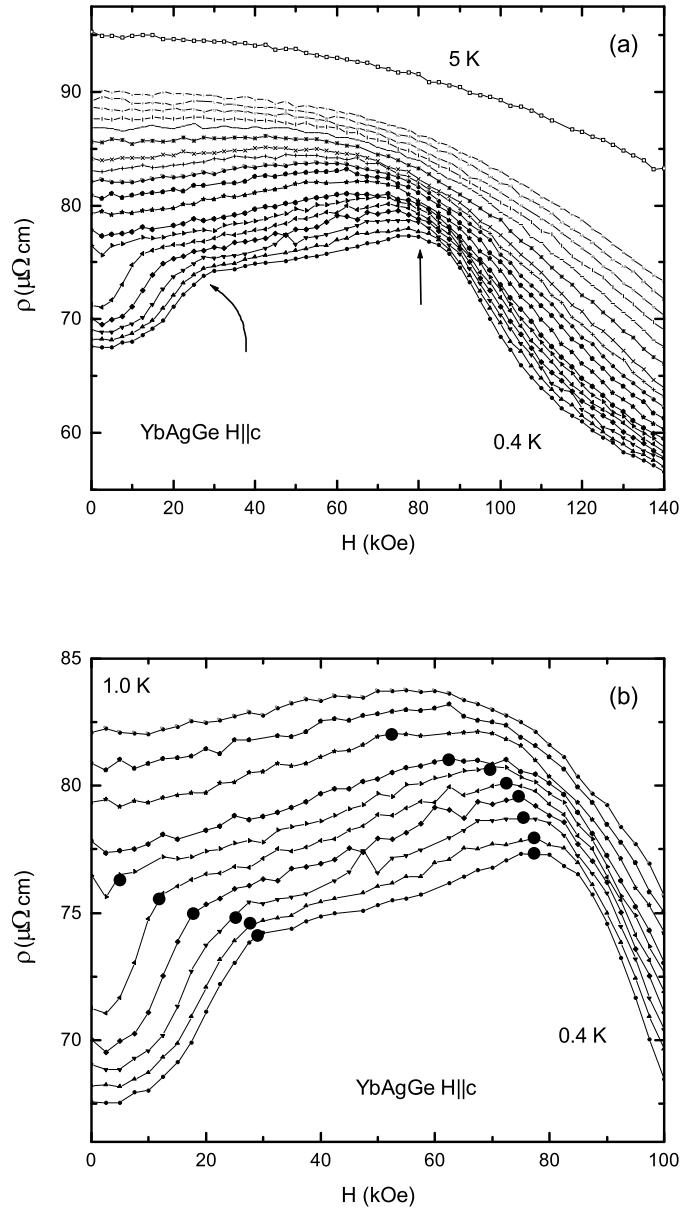


FIG. 7: (a) $\rho(H)$ ($H \parallel c$) isotherms for YbAgGe taken every 0.05 K between 0.4 K and 0.7 K, every 0.1 K between 0.8 K and 1.2 K, every 0.2 K between 1.4 K and 2.0 K and at 2.3 K, 2.5 K and 5.0 K, arrows point to the transitions discussed in the text; (b) enlarged low field - low temperature (0-100 kOe, 0.4-1.0 K) part of the panel (a), black dots mark transitions on the respective curves.

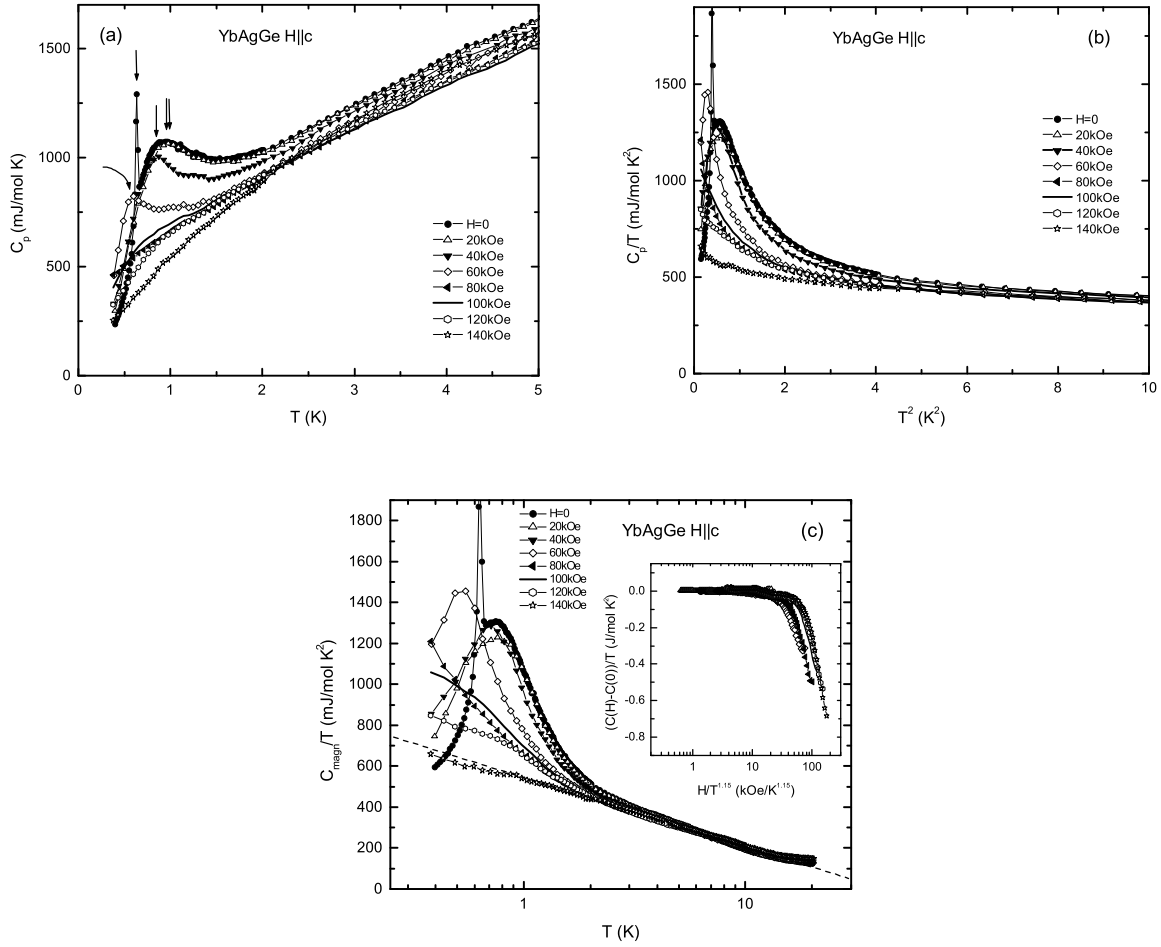


FIG. 8: (a) Low temperature part of the heat capacity curves for YbAgGe taken at different applied fields $H \parallel c$, arrows indicate peaks associated with magnetic ordering; (b) low temperature part of C_p vs T^2 curves; (c) semi-log plot of the magnetic part ($C_{\text{magn}} = C_p(\text{YbAgGe}) - C_p(\text{LuAgGe})$) of the heat capacity, C_{magn}/T vs T , for different applied magnetic fields, dashed line is a guide to the eye, it delineates linear region of the $H = 140$ kOe curve; inset: semi-log plot of $(C(H) - C(H = 0))/T$ vs $H/T^{1.15}$ ($T \geq 0.8$ K), note approximate scaling of the data for $H \geq 100$ kOe.

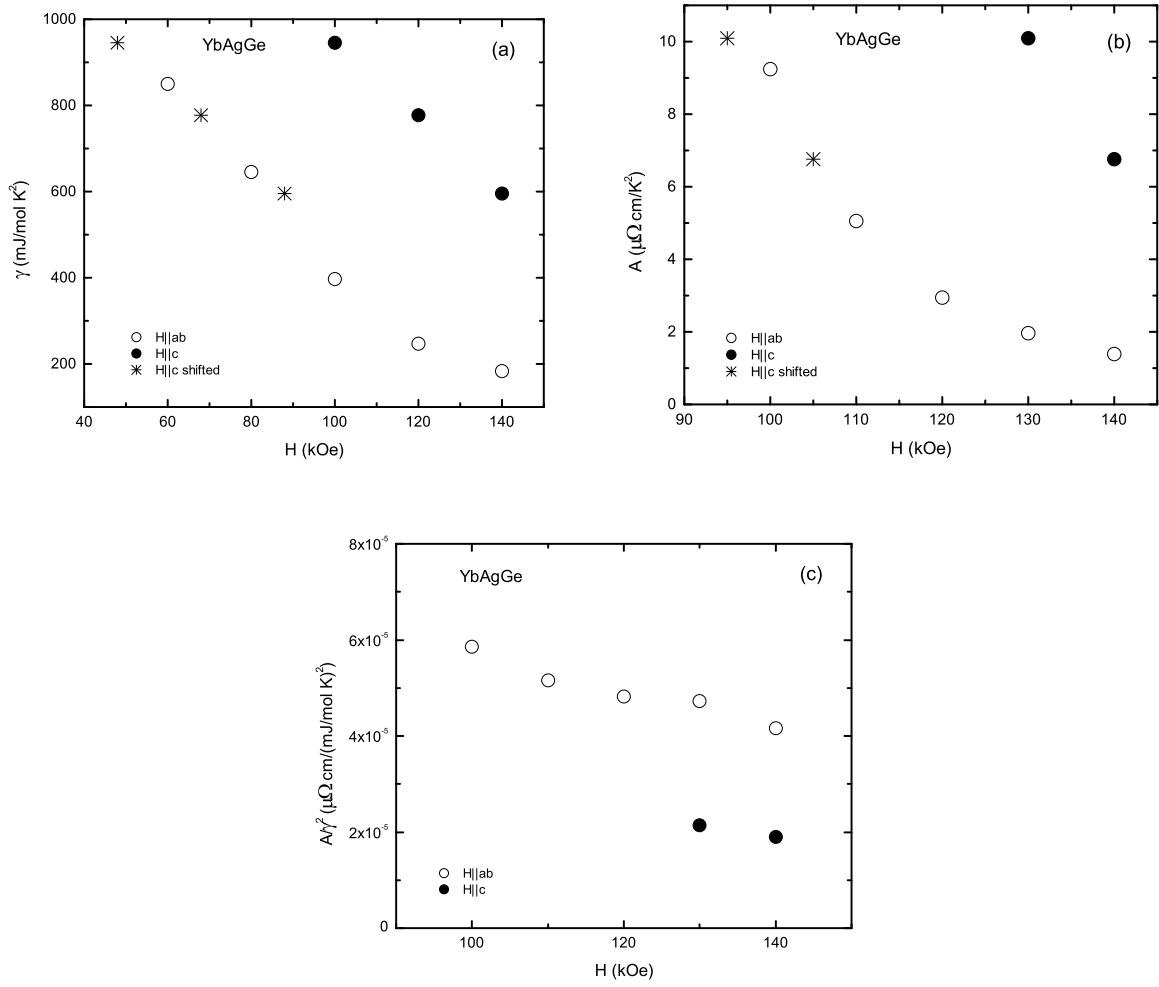


FIG. 9: The anisotropic field dependence of (a) the electronic specific heat coefficient γ ; (b) the resistivity coefficient A and (c) the Kadowaki-Woods ratio A/γ^2 . In figures (a) and (b) shifted data for $H \parallel c$ are shown as * (see text). The shift for figure (a) is -52 kOe and for figure (b) -35 kOe.

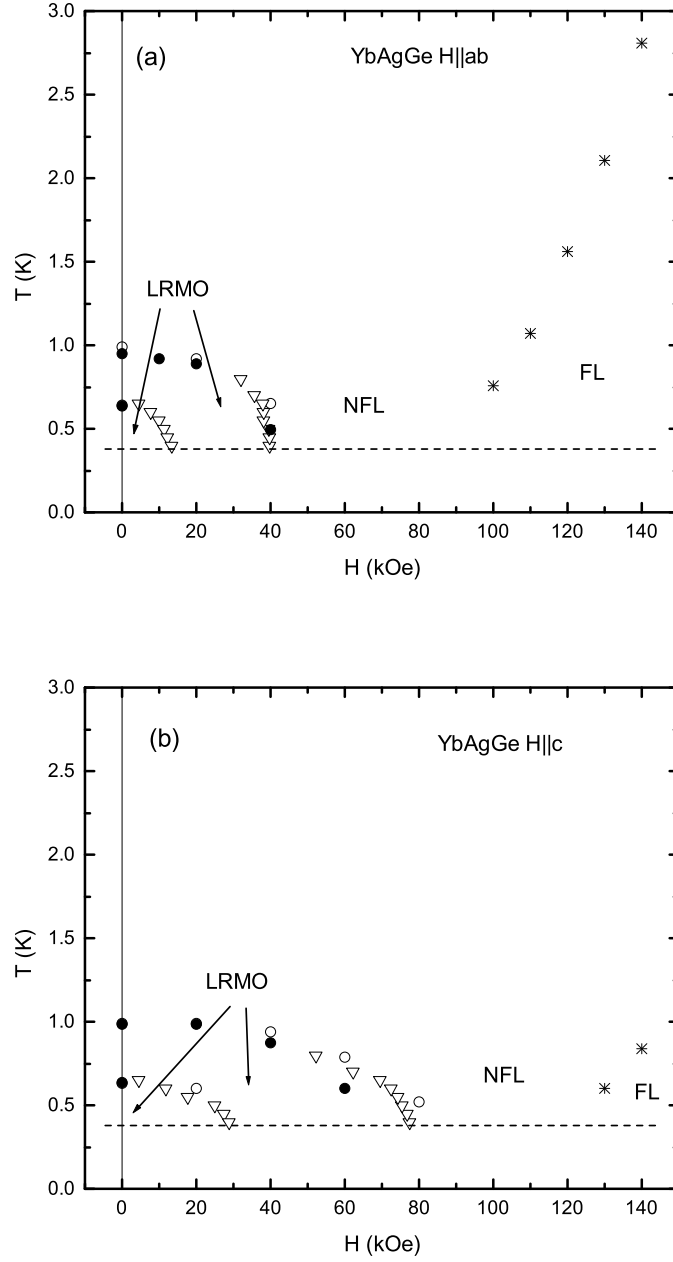


FIG. 10: Tentative $T - H$ phase diagram for (a) $H \parallel (ab)$; (b) $H \parallel c$. Long range magnetic order (LRMO), NFL and FL regions are marked on the phase diagram. Symbols: Filled circles - from $C_p |_H$ measurements, open circles - from $\rho(T) |_H$, open triangles - from $\rho(H) |_T$, asterisks - temperatures below which $\Delta\rho \propto AT^2$ in $\rho(T) |_H$ data (coherence temperature, T_{coh}). Dashed line - low temperature limit of our measurements, vertical line marks $H = 0$.